Rocket Project

December 8, 2014

Group Members:

Nathan Akers

Chad Bagley

Paul Campbell

Charles Juenger

Brian Mahan

Chris Skiba

Michael Weber

Michael Wermer

Advisor: Dr. Kareem Ahmed

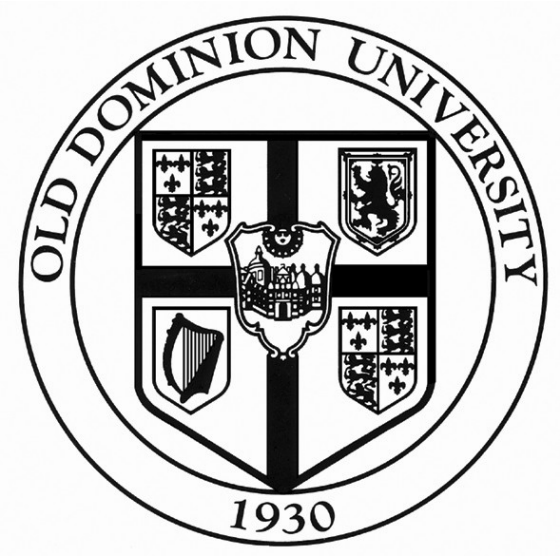

MAE 434W: 15725

Dr. Stacie Ringleb

Table of Contents:

Abstract: iii

Nomenclature: iv

Introduction: 1

Methods: 4

Completed Methods: 4

Proposed Methods: 9

FEA: 9

CFD: 10

Fuel Production: 11

Test Burns: 11

Wind Tunnel Testing: 12

Avionics Bay Assembly and Programming: 12

Vibration Analysis: 13

Preliminary Results: 15

Discussion: 17

Appendices: 19

Appendix 1: Figures 19

Appendix 2: Tables 29

Appendix 3: Budget and Budget Analysis 30

Appendix 4: Gantt Chart 33

References: 34

List of Figures:

Figure 1: Rocket Components……...……...……...……5

Figure 2: Rocket Assembly…….……...…….6

Figure 3: Combustion Chamber with converging-diverging nozzle……...……...…….8

Figure 4: Kn vs Web Regression……...……15

Figure 5: Chamber Pressure vs Time……..……...……15

Figure 6: Thrust vs Time……...……..……...……...……16

Figure 7: Nozzle Pressure and Temperature Distribution……..……...……16

Figure A1.1: Avionics Bay Components……...……...……19

Figure A1.2: Avionics Bay Dimensions ……...……...20

Figure A1.3: Nose Cone……...……....……21

Figure A1.4: Upper Rocket Body……..……...22

Figure A1.5: Lower Rocket Body...…….…….23

Figure A1.6: Rocket Fin…….....24

Figure A1.7: Rocket Motor Dimensions...…….25

Figure A1.8: Rocket Motor Components…….…….26

Figure A1.9: Motor Mount……...…….27

Figure A1.10: Nozzle Cone……...…...…….28

Figure A3.1: Cumulative Cost vs Weeks……...……32

List of Tables:

Table 1: Rocket Nozzle Dimensions and Variables……..17

Table A2.1: Published Values for Potassium Nitrate-Dextrose Fuel……..……..29

Abstract:

The design of a high-powered rocket capable of taking a cosmic ray detector payload to an apogee of 10,000 feet, deploying the payload, and recovering the rocket safely was created using computer aided drafting (CAD). Detailed designs of the structure, propulsion system, aerodynamic fins, avionics, and recovery system were developed. Structural stability will be determined through finite element analysis (FEA). The propulsion system will be powered by a potassium nitrate (KNO_3)-dextrose ($C_6H_{12}O_6$) solid propellant (KNDX) that will undergo combustion and expansion through a converging-diverging nozzle, delivering up to 5,120 Newton-seconds of impulse. The expected thrust for the fuel was calculated and an optimized nozzle was designed for the fuel. Aerodynamic analysis will be performed through modeled computational fluid dynamics (CFD) and validated through both, full-scale and scaled rocket wind tunnel testing to maximize airframe performance. The avionics system will autonomously record in-flight data and control the deployment of the payload, the drogue and main parachutes, ensuring safe recovery after flight. Fundamental vibration analysis will be performed to minimize in-flight vibrational effects on the payload and avionics system. All analysis and testing performed on the rocket will allow the team to extract as much information as possible to validate the design and ensure a safe and reliable flight.

Nomenclature:

r	Propellant Burn Rate
P_0	Combustion Chamber Pressure
K_n	Propellant Burn Area to Nozzle Throat Area Ratio
ρ_p	Propellant Density
P_{exit}	Nozzle Exit Pressure
P_{atm}	Atmospheric Pressure
M_{throat}	Nozzle Throat Mach Number
M_e	Nozzle Exit Mach Number
T	Thrust
V_{exit}	Nozzle Exit Velocity
$\dot{m}$	Mass Flow Rate
A^*	Nozzle Throat Area
D^*	Nozzle Throat Diameter
D_e	Nozzle Throat Diameter
R	Gas Constant
T_0	Combustion Chamber Temperature
γ	Ratio of Specific Heats
$\dot{m}$	Mass Flow Rate
X^*	Throat Position

Introduction:

Rockets are used to carry payloads into orbit, but are expensive and difficult to design. They need to be designed for the type, size, and weight of the payload to be carried. They need to be designed for the range to payload deployment. Four key areas need to be designed to fulfill the requirements necessitated by the payload. These include: structure, propulsions, aerodynamics, and avionics.

A high powered rocket is composed of cylindrical body, nose cone, avionics bay, tail fins, motor assembly, and recovery system. CAD software is used to create an accurate visual representation of the rocket and its components. The representation is used to perform analyses that determine design feasibility prior to construction [1]. CFD programs will utilize the three dimensional (3D) model to provide detailed information of flight aerodynamics. FEA is a method for determining stress and strain properties on complex solid bodies due to applied forces [2-4]. FEA is used on the rocket assembly to design for structural integrity and to verify material selection [5]. Both analyses will are needed to determine if the rocket design is capable of successful flight. Every new rocket design needs to be tested for structural integrity and stability.

Rocket motors are thrust engines, which operate by generating a pressure and momentum thrust; this is achieved by combusting fuel inside a pressure vessel and expanding the combustion products through a nozzle. This is typically accomplished in small-scale rockets by using solid rocket fuels. Commercially available “high-power” hobby rocket motors are typically made of Ammonium Perchlorate, HTPB and Aluminum, which is similar to the formulations used in rockets designed for space flight as well as missiles. These formulations, commonly referred to as APCP (Ammonium Perchlorate Composite Propellant), provide a high specific impulse relative to other solid formulations. Specific Impulse is a key concept in the design and

of a rocket motor because it is used to describe the efficiency of a fuel based on its weight. Specific Impulse is the ratio of the amount of thrust a fuel is able to produce to the weight flow of the propellants [6]. One drawback to using an APCP is the cost to produce; the material cost is high and the manufacturing process can be difficult. An alternative to APCP, which is commonly used in homemade rockets, is Potassium Nitrate-Sugar propellant, sometimes referred to as "R-Candy". This formula is easy to manufacture using readily available materials. The largest drawback to using these "R-Candy" formulations is the relatively low specific impulse they produce; meaning to reach a given altitude, more fuel is required. These formulations can be modified using different sugars such as sucrose, sorbitol, or dextrose, which can impact the material properties of the casted propellant as well as influence the ease of manufacturing as well as the reliability of the motor itself. While the general formulations are known, the amount of fuel and the types of quantities need to be modified in order to reach the target payload deployment altitude.

In order to achieve maximum propulsive efficiency, a rocket motor must sustain a high flow of heavy particles and elevated combustion temperatures while maximizing the speed of gases through the nozzle exhaust [7, 8]. Exponentially increasing temperatures in the combustion chamber can cause rapid deformation of the materials of the nozzle and chamber [7]. Combustion gas expansion induces high internal pressures within the combustion chamber, which further exacerbates component deformation. Gases that travel through the nozzle carry burnt aluminum particles, which cause ablation to the throat section of the nozzle and agglomeration in the nozzle cone [9-11]. This results in decreased efficiency by altering the nozzle inner dimensions. Additionally, heat transfer in the chamber must be controlled, as heat conducted through the chamber walls results in heat loss to the combustion gases [12]. The

inability to accommodate these operating conditions results in performance inefficiencies as well as potential component failure. Determination of a nozzle design, which accommodates maximum operating conditions, will increase performance and longevity while reducing cost. The nozzle dimensions must be individually designed for every rocket because of unique fuel composition.

Aerodynamics is examined to reduce drag and shock effects. Shapes of nose cones and fins have been examined in an effort to reduce drag and shock effects [13-18]. Nose cone designs showed that increased ratios of nose cone length to body length decreased drag, and reduction of the angle of the nose cone resulted in a smaller shock transition between the nose and the rocket body during supersonic flight [14, 15]. Fin designs were primarily focused on the flight stability, but as the size and bluntness of the leading edge increased, the drag and shock effects increased [13,16-18]. While the basic aerodynamics of fins and nose cones are known, the final fin designs and nose cone designs are modified for every rocket based upon mass, length, and expected flight velocities.

The avionics bay of a model rocket is typically positioned in the center section of the rocket, between the forward nose cone and rear motor section. The avionics bay must be designed to protect the rocket's sensitive electronics, both from in-flight forces and impact from landing. The National Aeronautics and Space Administration (NASA) identifies four in-flight forces: weight, thrust, lift and drag [19]. The avionics bay must be designed to properly house and support the sensitive electronics, and mitigate the damaging effects from these in-flight forces. A rapid shock is an additional force the rocket could experience upon landing. The purpose of the parachute recovery system of the rocket is to lessen this shock load. The electronics mounting and structural design of the avionics bay must account for both the in-flight

forces and the shock load upon landing. The maximum in-flight forces and shock load are unique to every rocket because every rocket has a different thrust which affects the in-flight forces and a different mass which affects the shock load.

Altimeters are devices used to measure the altitude by measuring the change in pressure. Many of the operating principles used in rocketry altimeters have remained relatively the same. The avionics system needs to contain an altimeter that will control the ejection of the payload, as well as the parachute recovery system, allowing for the rocket and payload to be safely recovered.

The onboard avionics system allows for the collection of performance data, which determines the in-flight characteristics of the rocket. This data can be compared to theoretical and simulated analytical data to determine if the rocket performed as expected. Using the comparison, needed adjustments can then be made to the design to maximize the rocket's performance. Therefore, the purpose of this project was to design a reusable high-powered rocket capable of deploying a five pound cosmic ray detector at 10,000 feet by designing the structure, propulsion system, and avionics section.

Methods:

Completed Methods:

A 3D model of the rocket was created using Autodesk Inventor (Autodesk Inc., San Rafael, CA) and was developed by designing part assemblies of the different rocket components. These components (Figure 1) were then joined together to produce the main rocket assembly (Figure 2).

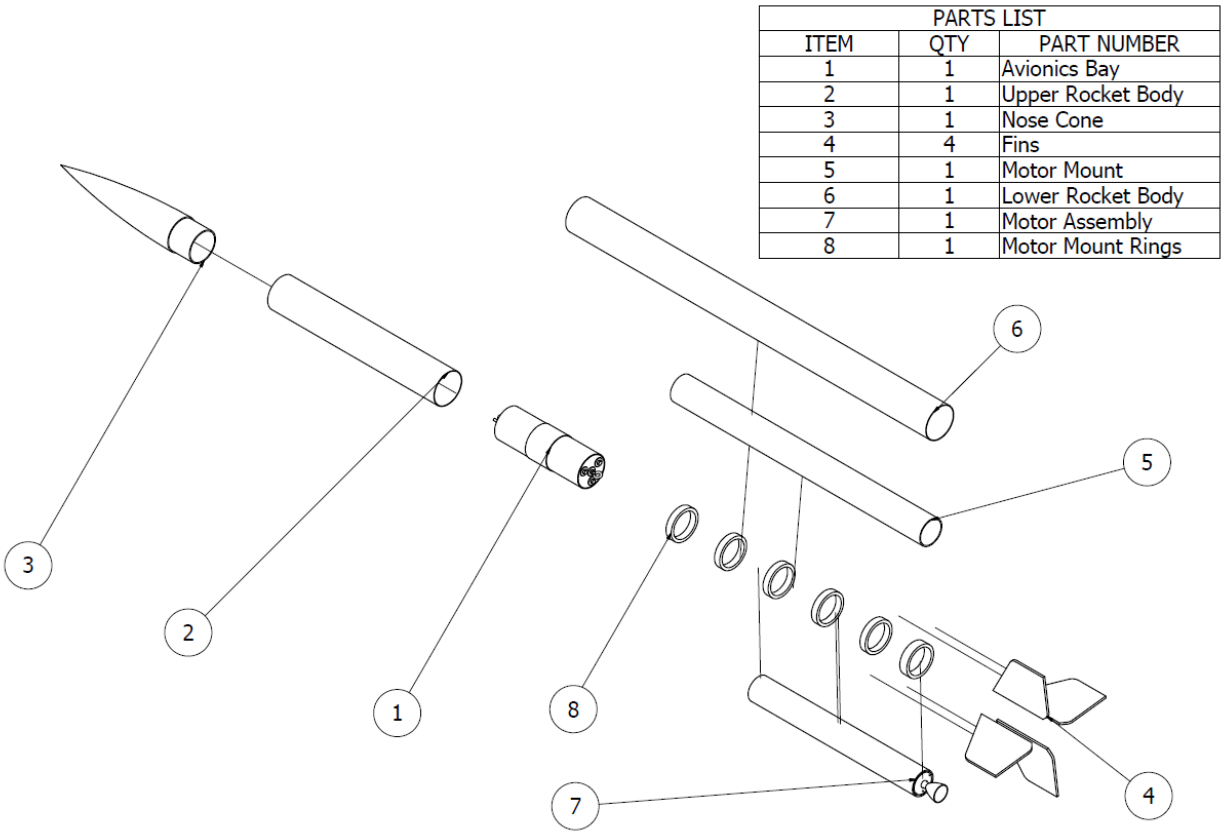

Figure 1: Rocket Components

The first part assembly to be designed was the avionics bay (Figure A1.1- A1.2), which will house the electrical equipment and connect the top and lower portions of the rocket. The ends were fitted with two circular end caps and were secured to the tubular housing by three bolts with accompanying fastener hardware. Eyebolts were then fitted to the center of the two end caps by fasteners. These bolts will serve as an anchor point for the shock chords after in flight rocket separation has occurred. The nose cone (Figure A1.3) was designed with a hollow cavity surrounded by the nose cone walls. A circular end cap with a U-bolt and the accompanying fasteners were fitted to the end of nose cone. The U-bolt will serve as another anchor point for the top shock chord. Connecting the nose cone and the avionics bay is the upper rocket body (Figure A1.4). The lower rocket body (Figure A1.5) consisted of a tube that was fitted with four triangular fins (Figure A1.6) designed by the aeronautical branch. The engine assembly was

designed to maximize propulsive efficiency, and this assembly was made up of a nozzle, outer casing, resin liner and end cap (Figures A1.7-A1.8). This was attached to the lower rocket body via six circular motor mounts (Figure A1.9) attached to inner walls of the bottom rocket body.

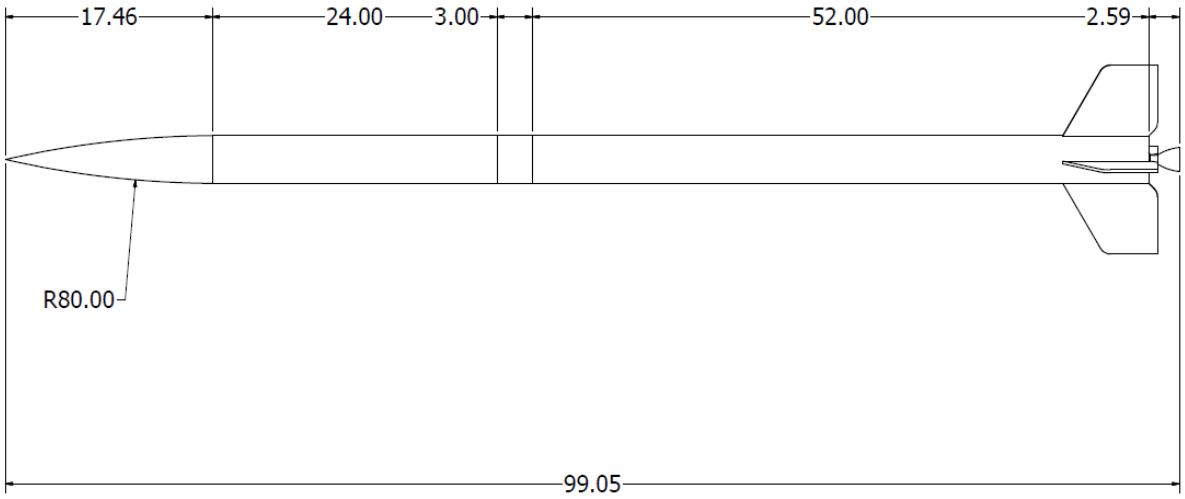

Figure 2: Rocket Assembly

The rocket is to be powered by an "experimental" fuel, meaning that the motor is to utilize a homemade propellant formulation in lieu of a commercially available motor. The formulation was taken from Richard Nakka's Experimental Rocketry Website [20]. The need to select a pre-investigated formulation was necessitated by the compressed budget and timeline of this project as there were not enough resources available to develop a unique formulation which could function safely and reliably. The propellant selected for this project was a mixture of 65% by mass Potassium Nitrate (KNO_3) and 35% by mass Dextrose ($C_6H_{12}O_6$) and is seen below [21].

$$C_6H_{12}O_6 + 3.31\ KNO_3 \rightarrow 2.116\ CO_2 + 2.300\ CO + 4.512\ H_2O + 1.424\ H_2 + 1.655\ N_2 + 1.585\ K_2CO_3 + 0.133\ KOH \quad \text{(Equation 1)}$$

(theoretical combustion reaction at 68atm [21])

This formulation was tested extensively and is commonly used by high-power rocketry hobbyists. This relatively inexpensive formula has been proven to be safe and reliable while being relatively easily manufactured, and produces results within a reasonable margin of predicted results calculated by using the published values (Table A2.1). A preliminary motor design was developed using a "freeware" Microsoft Excel (Microsoft Corporation, Redmond, WA) spreadsheet ("SRM_2014") published by Richard Nakka [22] to target a maximum operating pressure within the combustion chamber of 1100psia. This target pressure was based off a preliminary motor casing design, to be constructed from 2.95" outside diameter, 6061-T6 Aluminum tubing with a wall thickness of 0.11", giving an inside diameter of 2.73". The selected pressure of 1100psia used a conservative factor of safety of 2, this conservative value was selected because of the need to re-use the motor casing multiple times and the relatively low-impact of the casing weight on the rocket performance and design. The size of our motor was scaled to deliver as close to 5120 Newton-seconds of impulse as possible, without exceeding that limit. The desired pressure is achieved by modifying the "K_n" value, which is the ratio of burning surface area of the propellant to the area at the throat of the nozzle [23]. This was done by selecting a commercially available propellant casting mold and modifying the nozzle diameter to meet the required "K_n" value.

The nozzle (Figure 3) was assumed to be isentropic, and compressible flow equations were used to determine the thermodynamic properties at the subsonic, sonic, and supersonic regions. The properties at each station and the constraint of three inches on the converging

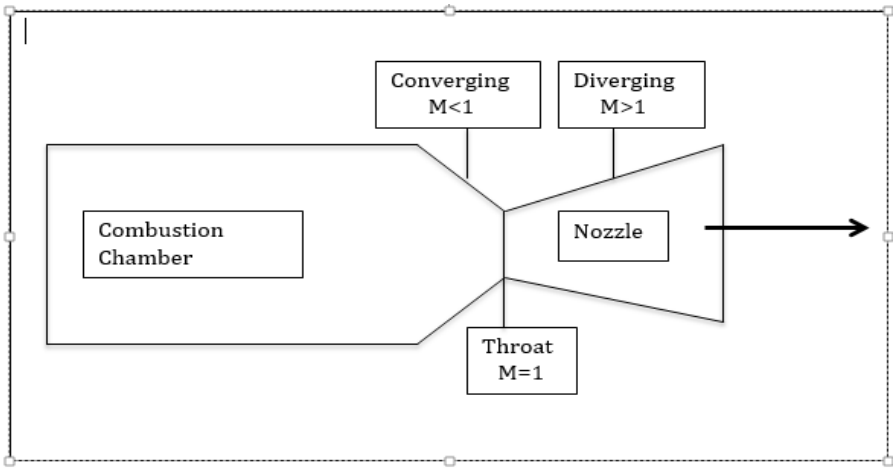

Figure 3: Combustion Chamber with converging-diverging nozzle

section were used to determine the dimensions of the nozzle. To reach maximum propulsive efficiency, the exit gases must be expanded through the diverging section of the nozzle so that P_{exit} equals P_{atm}. The mass flow rate in the nozzle was determined by $\dot{m} = \frac{Thrust}{V_e}$ (Equation 2) where $V_e = \sqrt{\frac{2\gamma RT_c}{\gamma - 1}\left[1 - \frac{P_e}{P_c}\right]^{\frac{\gamma-1}{\gamma}}}$ (Equation 3). Using the mass flow rate and exit velocity, the throat diameter was determined using the equation $D^* = \sqrt{\frac{4\dot{m}\sqrt{RT_c}}{\pi P_c X^*}}$ (Equation 4) and X^* is a function of the ratio of specific heats $X^*(\gamma) = \sqrt{\gamma}\left(\frac{2}{\gamma+1}\right)^{\frac{\gamma+1}{2(\gamma-1)}}$ (Equation 5). Next, the nozzle exit diameter was found by first finding the Mach number at the exit by $M_e = \sqrt{\frac{2}{\gamma-1}\left[\left(\frac{P_c}{P_e}\right)^{\frac{\gamma+1}{2(\gamma-1)}} - 1\right]}$ (Equation 6). Substituting the Mach number into the equation for area ratios provided the diameter for the exit $D_e = \sqrt{A^* \frac{4}{\pi}\left(\frac{1}{M_e}\left[\left(\frac{2}{\gamma+1}\right)\left(1 + \frac{\gamma-1}{2}M_e^2\right)\right]^{\frac{\gamma+1}{2(\gamma-1)}}\right)}$ (Equation 7). A simulation of the nozzle was run at the determined area and pressure ratios using the CD Nozzle Simulator (engApplets, Blacksburg, VA).

The software chosen to perform CFD analyses on the fins and nose cone was Simulation CFD (Autodesk Inc., San Rafael, CA). The assumptions for the flow to be used in the CFD analyses were a fluid of air, compressible flow, sea level standard air conditions, steady flow, and no heat transfer. The inputs were Mach number and angle of attack. The output criteria to judge the different designs were coefficient of drag and center of pressure. The preliminary rocket nose cone length to body length ratio was 0.18.

Proposed Methods:

FEA:

The FEA will be carried out through the application of NASTRAN In-Cad (Autodesk Inc., San Rafael, CA). The test to be performed will consider the motor assembly and the stress put on it from thrust. The maximum thrust force limit of 5120 Newtons will be applied to the rocket nozzle. The material properties for the motor mount and engine assemblies will entered into the software. Two separate analyses will be conducted using different constraints around the motor mount. The first constraints will be applied to the circular struts around the motor mount. The force of these constraints will be determined from the strength of different glues under consideration. The next constraint to be tested will be the bolts securing the nozzle to the outer casing of the engine. The strength of this constraint will be determined from the metallic properties of the bolts. A 3D mesh of the motor mount and engine will be created and the FEA will be run. The results will be recorded in the form of a Von Mises stress plot and an animated displacement plot. This analysis will determine if the appropriate amount of struts and bolts were designed for to prevent structural failure from thrust using a nominal factor of safety of one. Additionally, NASTRAN In-Cad (Autodesk Inc., San Rafael, CA) and FEA will be used to simulate heat and dynamic loads through the nozzle. This will provide high-resolution analysis

of heat transfer and stress at operating conditions. The results will be used to confirm the materials selections, of graphite for the nozzle and aluminum for the combustion chamber.

CFD:

A minimum of eight fin designs will be created using Autodesk Inventor (Autodesk Inc., San Rafael, CA). They will be the same general shape as the fins on the preliminary rocket design. The eight fin designs will be created by changing one parameter on the original preliminary fin design, while holding all other dimensions constant. The parameters will be height, length, thickness, and angle of incline. Two designs will be created for each parameter by changing the parameter to 75% and 125% the size of the preliminary design. Each new design and the original will then be run through Simulation CFD (Autodesk Inc., San Rafael, CA) at Mach numbers of 0.5, 0.8, 1.0, 1.2, and 1.5, and final fin design created based upon results. Additionally, a minimum of four nose cone designs will be created. The only parameter that will be changed to create the designs is the nose cone length to body length ratio. The four new designs will use ratios of 50%, 75%, 125%, and 150% the magnitude of the preliminary design ratio. These four designs and the preliminary design will be run through Simulation CFD (Autodesk Inc., San Rafael, CA) at Mach numbers of 0.5, 0.8, 1.0, 1.2, and 1.5. Based upon the results of these analyses the final nose cone design will be chosen.

Once the final nose cone and fin designs are chosen, CFD analyses will be run on the entire rocket body using the chosen nose cone and fin designs. The analyses of the rocket body will be done from 0.1 to 1.5 Mach in steps of 0.1 and from 0 to 16 degrees angle of attack in steps of 2 degrees. In total there will be a total of 135 analyses. From this data an aerodynamic properties report will be created.

Fuel Production:

The process of manufacturing the fuel requires the two components to be thoroughly mixed together and then heated until the dextrose melts, homogenously binding the two products together. The particles must be desiccated and finely milled before mixing and heating to ensure the maximum performance of the propellant; errors in manufacturing can cause results which are significantly less than what is predicted. The particles will be mixed together using a rotating drum or other low-speed mixture to ensure an evenly distributed mixture. The dextrose will fully melt at 123°C [20], in order to create the propellant; the particle mixture will be heated between 125-130°C. The sugar will begin to caramelize at 157°C [20] so it is important to use a calibrated hot plate to precisely control the temperature; caramelization of the sugar will negatively impact the performance of the propellant. While heated, the mixture will be packed into a 2.562" inside-diameter, cylindrical casting tube, placed around a cylindrical core with a diameter of 0.6875". To form the motor, six of these castings will be made at a length of 4.83"; each of these castings is known as a grain. The completed motor will be comprised of six grains, totaling 28.98" long with an outside diameter of 2.562", and a core diameter of 0.6875", for a total volume of 132in^3.

Test Burns:

A one forth scale model of the completed motor will be test fired before the final motor is machined. Pressure will be measured using a PX-303 load cell (Omega, Stamford, Connecticut) and the thrust data is measured using a PX-LCJA (Omega, Stamford, Connecticut). The data will be collected from the static test using a DI-194 (DATAQ Instruments, Akron, OH). The data from this test will be used to validate the software simulations and used to adjust the fuel component percentages.

Wind Tunnel Testing:

Subsonic and supersonic wind tunnel testing will be conducted after the CFD modeling. The subsonic testing will use the assembled rocket body and the supersonic testing will use a scale model of dimensions that are to be determined, so that supersonic flow is accurately modeled. Data will be collected using a pressure sensor. This data will be compared to the CFD modeling to determine its accuracy.

Avionics Bay Assembly and Programming:

The avionics system will consist of a telemetry device, parachute ejection system and power supply. The telemetry device, TeleMetrum (Altus Metrum, LLC), is compact and measures 2.75 inches long and 1 inch wide [24]. TeleMetrum will contain a single axis, 70-g (+/-) accelerometer, and a dual-deployment altimeter good for atmospheric pressure measurements up to 45,000 feet [24]. The altimeter will be programmed to deploy two separate parachute ejection charges that will allow failure of the rocket airframe shear pins. The ejection charges and airframe shear pins will be sized using common rocketry calculators [25]. The first ejection charge will cause shear pin failure of the rocket's forward airframe and will release the drogue parachute and cosmic ray detector payload. The drogue parachute will be deployed at the rocket's apogee and used to decelerate and stabilize the descent of the rocket. The second ejection charge will cause shear pin failure of the rocket's rear airframe and will deploy the main parachute at approximately 800 feet above the ground.

TeleMetrum will provide Global Positioning System (GPS) tracking, including a 70-cm band transmitter allowing for real-time flight data analysis [24]. Flight data will be transmitted to a launch site laptop computer using the device's supplied software and antenna hardware connector. A handheld Yagi-Uda antenna will be used to detect the transmitter's high frequency.

TeleMetrum will be powered by a 900 mAh, rechargeable Lithium-Ion Polymer (LiPo) battery [24]. TeleMetrum will consume approximately 150 mA during a typical flight and the larger power capacity will allow for multiple rocket flights without the need to recharge [24].

TeleMetrum and associated power supply will be located inside of the rocket's avionics bay. The components will be mounted to a plywood sled using nylon mounting posts, rubber vibration isolators, screws and tie-wraps. The sled will be approximately 12 inches in length, oversized to allow the transmitter radio antenna to be fully unfolded. The avionics bay will contain an external power switch, mounted to the airframe and wired to TeleMetrum. The switch is a safety device and will allow the device to be manually energized from the outside of the airframe prior to launch, preventing accidental ejection charge activation during prelaunch setup. TeleMetrum software will aid in the testing and analysis of the rocket's flight. Data will be transmitted from TeleMetrum to a launch site laptop computer allowing the rocket operator to track the performance of the rocket. Over 40 separate downloadable data will be collected and will be used to analyze the performance of the rocket [24].

Vibration Analysis:

Vibration damping analysis will deliver the information needed to provide protection from structural vibrations during the rocket's flight. The avionics bay will be modeled as a single-degree-of-freedom system. It will act under forced vibrations showing that the vibration frequency will follow the frequency of the rocket motor. The fundamental equation governing vibration frequency is $f_n = \frac{1}{2}\pi\sqrt{k/m}$ (Equation 8). Since it is not practical to perform actual bench testing to analyze the vibration analysis, theoretical vibration analysis will be conducted using Autodesk Simulation Mechanical (Autodesk Inc., San Rafael, CA). This software will allow a theoretical vibration load to be applied to the avionics bay assembly that was previously

modeled in Autodesk Inventor. After the theoretical analysis, in order to mitigate the effects of vibration on the rocket avionics section, a soft pliable rubber to isolate the avionics sled will be used. The rubber will be attached to the corners of the sled where contact is made between the rocket structures.

While also conducting vibration analysis, the deployment force of the parachute will be calculated to ensure the snatch force applied does not damage the rocket structure. During parachute deployment the lines first method will be used to minimize the tension (snatch force) applied to the rocket [26]. This allows the rocket to initially slow as the lines are released and then the parachute is fully deployed as the lines pull the parachute out of the body. To ensure the stress will not be too high for the rocket structure, snatch force calculations will be performed to measure the amount of tension generated during deployment. The corresponding tension (snatch force) is found using $P = nK'[\frac{\{1-(1+4A)^{0.5}\}}{2r_p} + \frac{Vr}{c}]$ (Equation 9).

Preliminary Results:

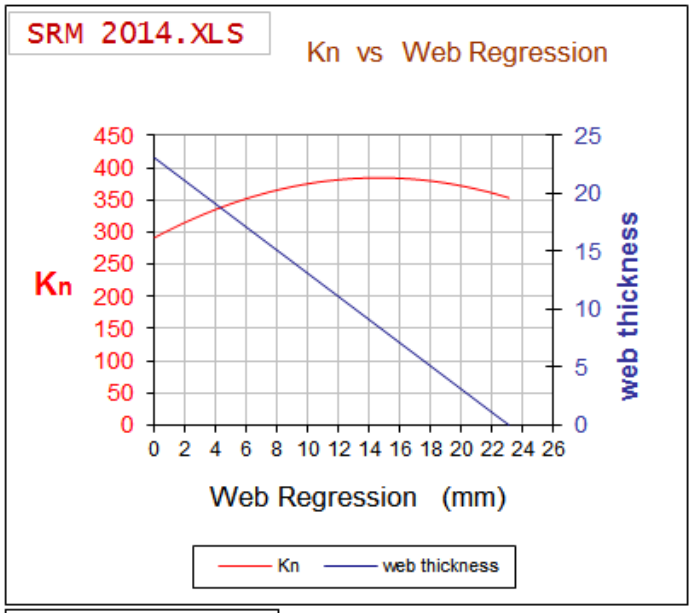

Figure 4: Kn vs Web Regression

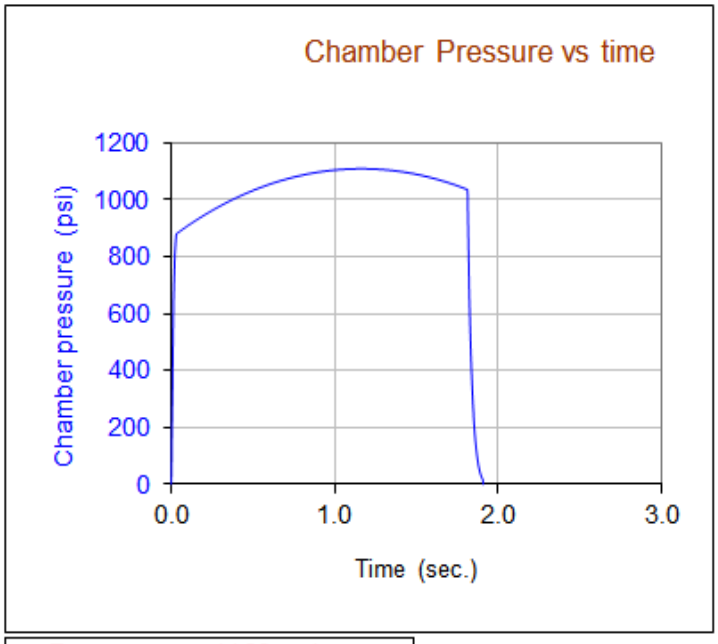

Figure 5: Chamber Pressure vs Time

A preliminary rocket design was completed based upon commercial rocket designs. These include the nose cone, avionics bay, rocket outer body, motor mount, fins and engine (Figure 1).

The rocket fuel propellant was chosen from a formulation commonly used by rocketry hobbyists. Using this fuel the combustion chamber pressure reached the desired value of 1100psia given a factor of safety of 2. Additionally, 5120 Newton-seconds of impulse was achieved by analyzing the "K_n" value. In the simulation the rocket propellant burned progressively in from the center core, causing the exposed surface area to increase (Figure 4), to a maximum "K_n" value of 384, resulting in a max pressure in the chamber of 1109psia (Figure 5). The motor as it is

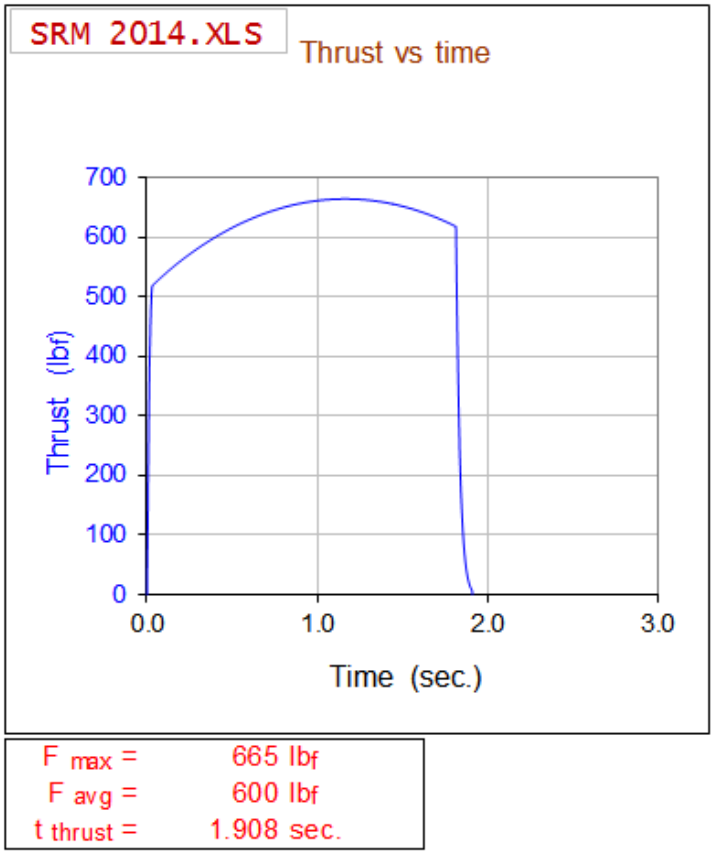

Figure 6: Thrust vs Time

velocity of 977 feet/sec.

During nozzle design, analysis was conducted to ensure no shock waves formed inside the nozzle. This simulation analysis shown (Figure 7) revealed no shock waves forming inside the nozzle that will decrease propulsive efficiency.

The combustion chamber peak pressure results can be seen below (Table 1). This pressure range was used to determine the

currently designed will produce thrust for 1.908 seconds (Figure 5) at an average thrust of 2671 Newtons (Figure 6). This configuration will deliver a total impulse of 5096.8 Newton-seconds, which is 99.5% of our target impulse. With an estimated empty-weight for the rocket of 30 pounds and estimated drag coefficient of 0.45, this motor configuration will take the rocket to an altitude of 10,275 feet in 24.5 seconds, with a max

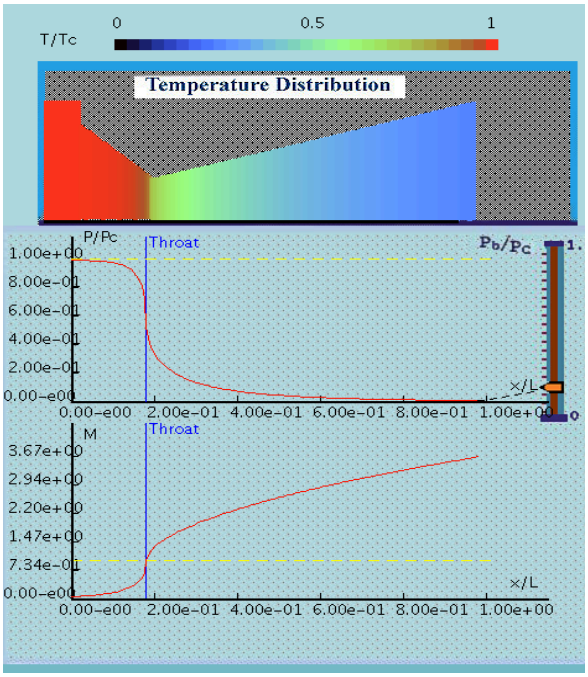

Figure 7: Nozzle Pressure and Temperature Distribution

approximate properties at the inlet, throat, and exit of the nozzle. The optimal nozzle dimensions and conditions were determined and shown in the appendix (Figure A1.10).

Rocket Nozzle Data			
	Inlet	Throat	Exit
Diameter (m)	0.06096	0.015875	0.05715
Area (m2)	0.00292	0.00020	0.00257
Mach		1	3.24
Velocity (m/s)		598.96	1539
Pressure (kPa)	7800	4519	101.34
Temperature (K)	1625	1525	983.23
Gamma	1.1308	1.1308	1.1308
mdot (kg/s)	2.02	2.02	2.02
Expansion Ratio	12.96		
Thrust (N)	3100		
Gas Constant (kJ/kg-k)	208		

Table 1: Rocket Nozzle Dimensions and Variables

Discussion:

The purpose is to design and build a rocket capable of getting to 10000 feet carrying a cosmic ray detector, deploy the cosmic ray detector, and return safely. The electronics were chosen, the fuel analyzed, the design model created, and the recovery system chosen. However, it is unknown whether the preliminary design is structurally and aerodynamically stable.

The size of the motor was scaled to deliver as close to 5120 Newton-seconds of impulse. The desired pressure was achieved by modifying the "K_n" value. This was done by selecting a commercially available propellant casting mold and modifying the nozzle diameter to meet the required "K_n" value. Before ignition, the "K_n" value was 291; this was favorable because a higher "K_n" value allows for more reliable ignition. The Potassium Nitrate-Dextrose propellant, sometimes referred to as "R-Candy" is easy to manufacture using readily available materials.

The largest drawback to using these “R-Candy” formulations is the relatively low specific impulse they produce. These formulations can be modified using different sugars such as sucrose, sorbitol, or dextrose, which can impact the material properties of the casted propellant as well as influence the ease of manufacturing and the reliability of the motor itself.

A number of limitations are inherent in the calculations done in the fuel analyses, rocket nozzle design, and future CFD analysis. The fuel analyses used published property values which will differ slightly in the final formulation due to modifications that will be made based upon the test burn data. The combustion analysis assumes infinite combustion area and frozen flow. This simplifies the calculations but adds some error to the results. The nozzle design is optimized for the maximum pressure which occurs at takeoff and would not demonstrate pressure equal to ambient pressure during other parts of the flight. The CFD analysis assumes sea level conditions, and this will only be valid part of the time because the conditions change as the rocket increases in altitude. Additionally, the material assumed for the rocket body is not correct so the predicted skin friction used in the total drag will be slightly different from the actual.

Future work will include FEA, CFD analysis, vibration analysis, wind tunnel testing, and rocket engine testing to determine the validity of the design. A full flight cannot be done until the cosmic ray detector is built by the physics team and delivered.

Appendices:

Appendix 1: Figures

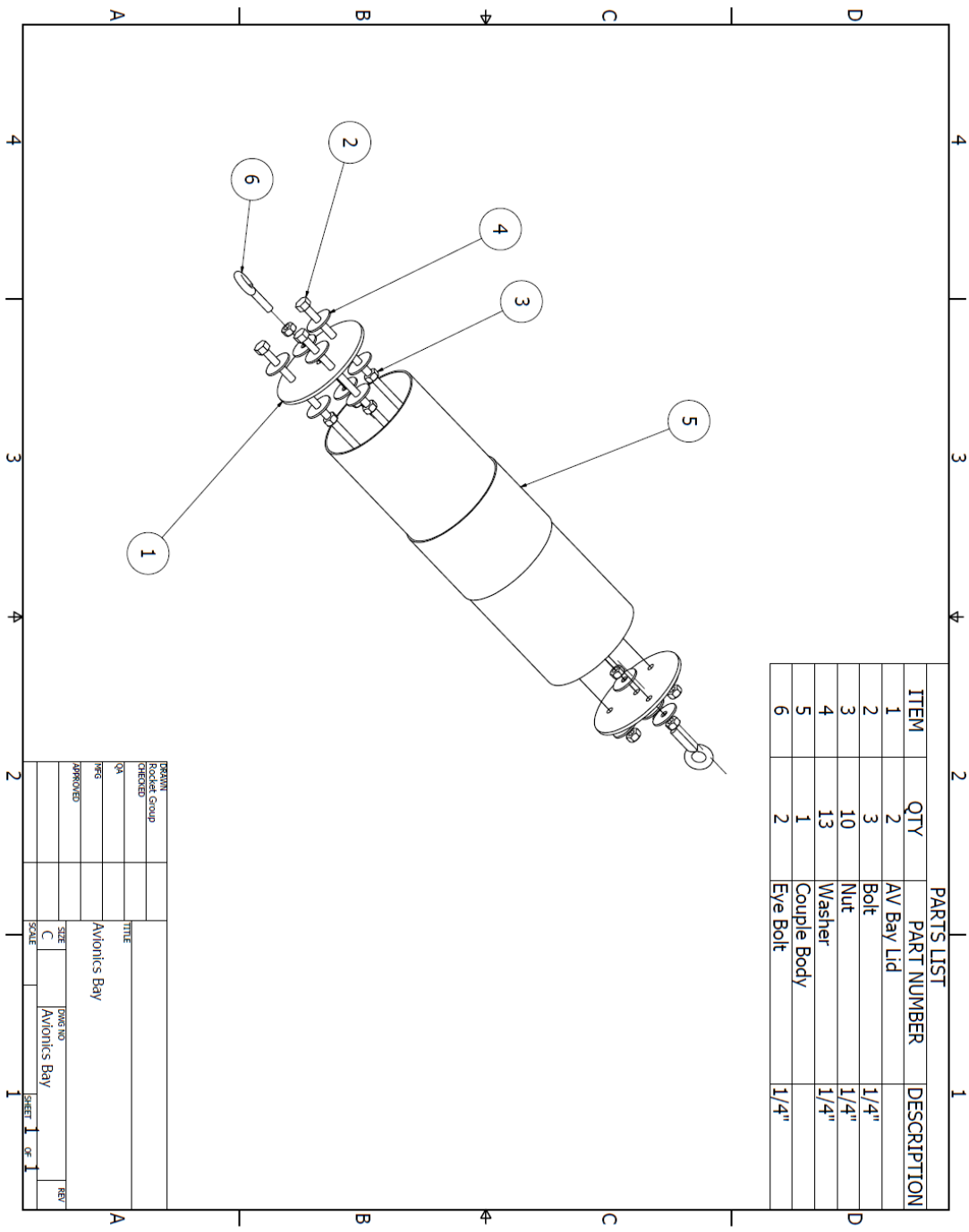

Figure A1.1: Avionics Bay Components

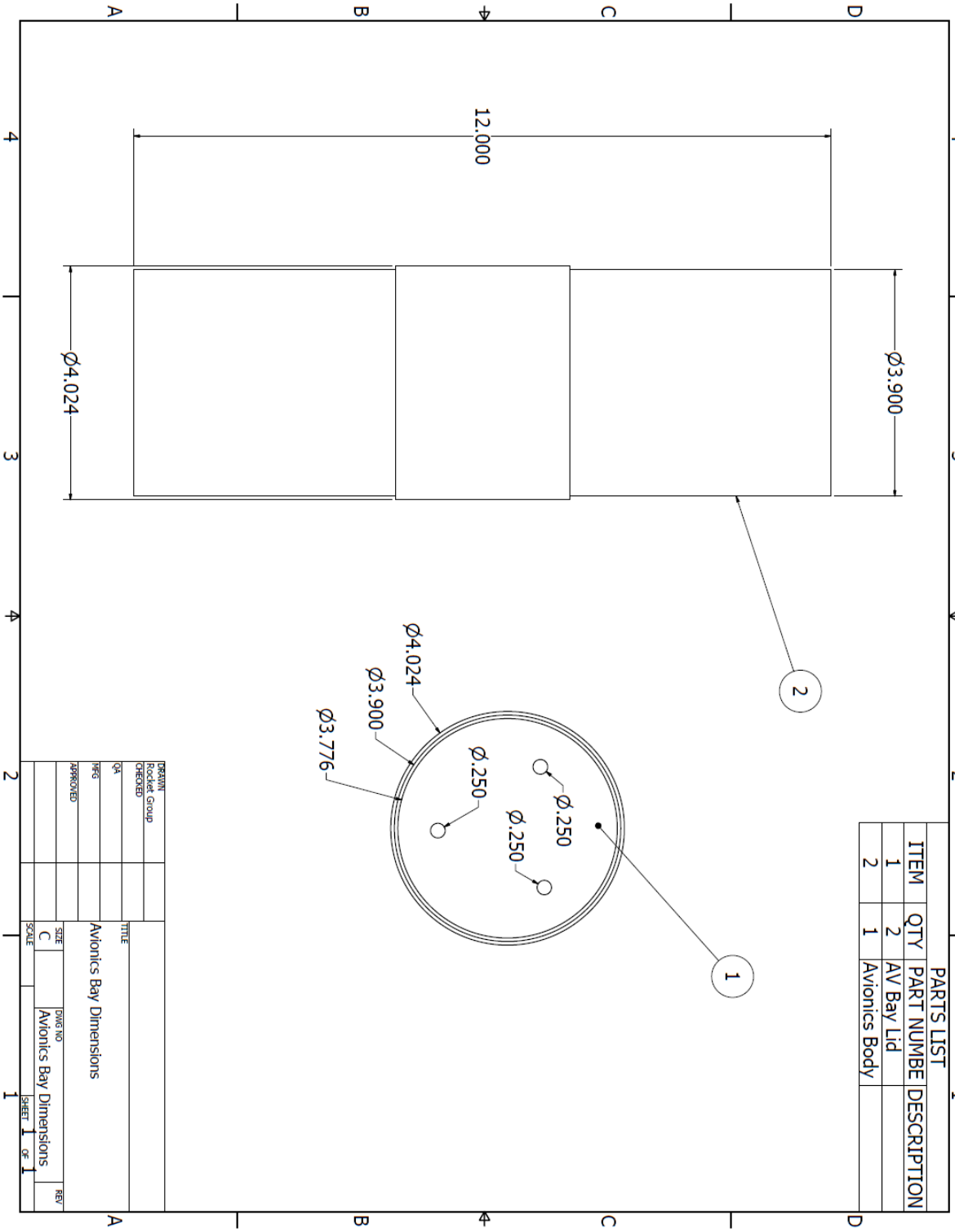

Figure A1.2: Avionics Bay Dimensions

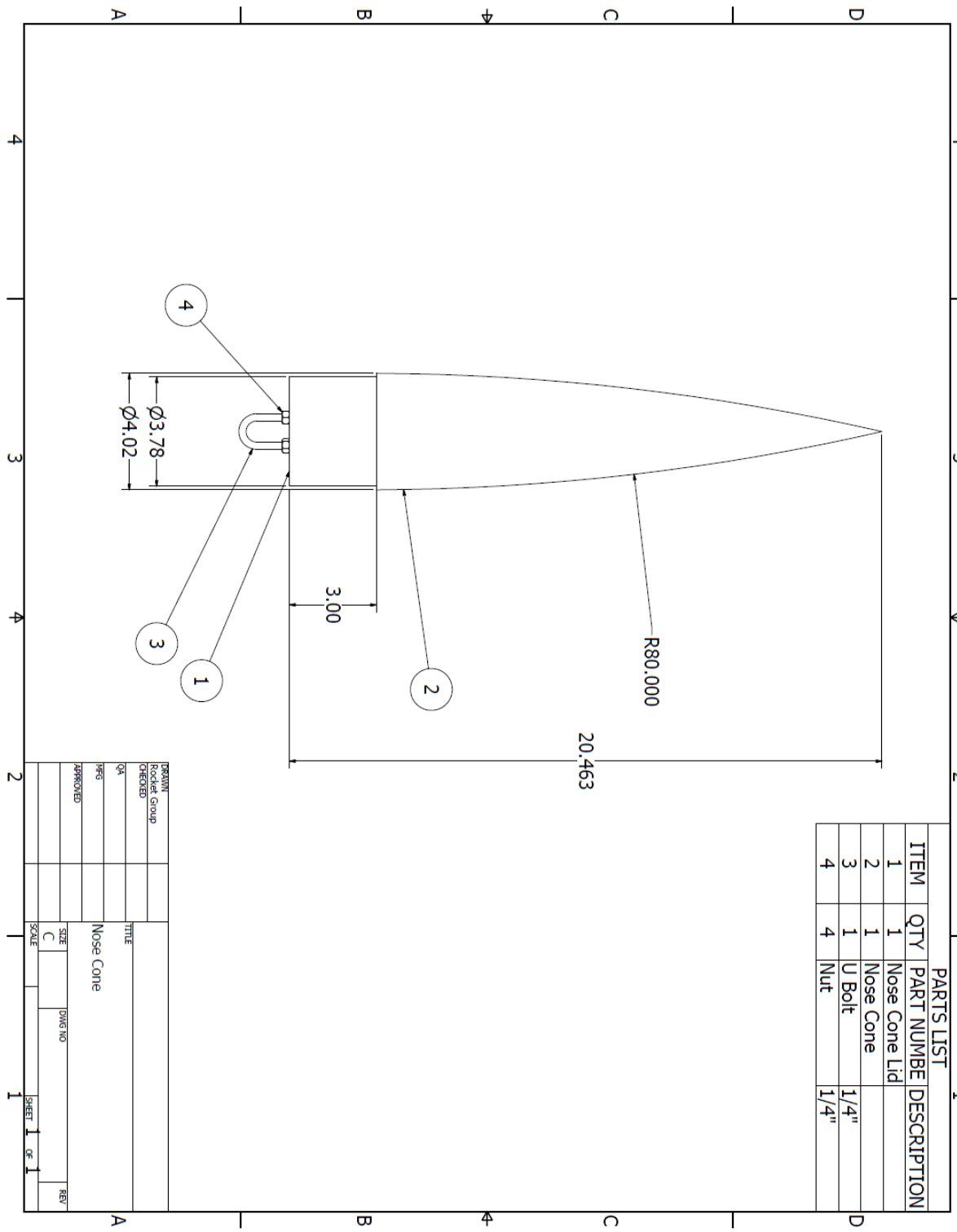

Figure A1.3: Nose Cone

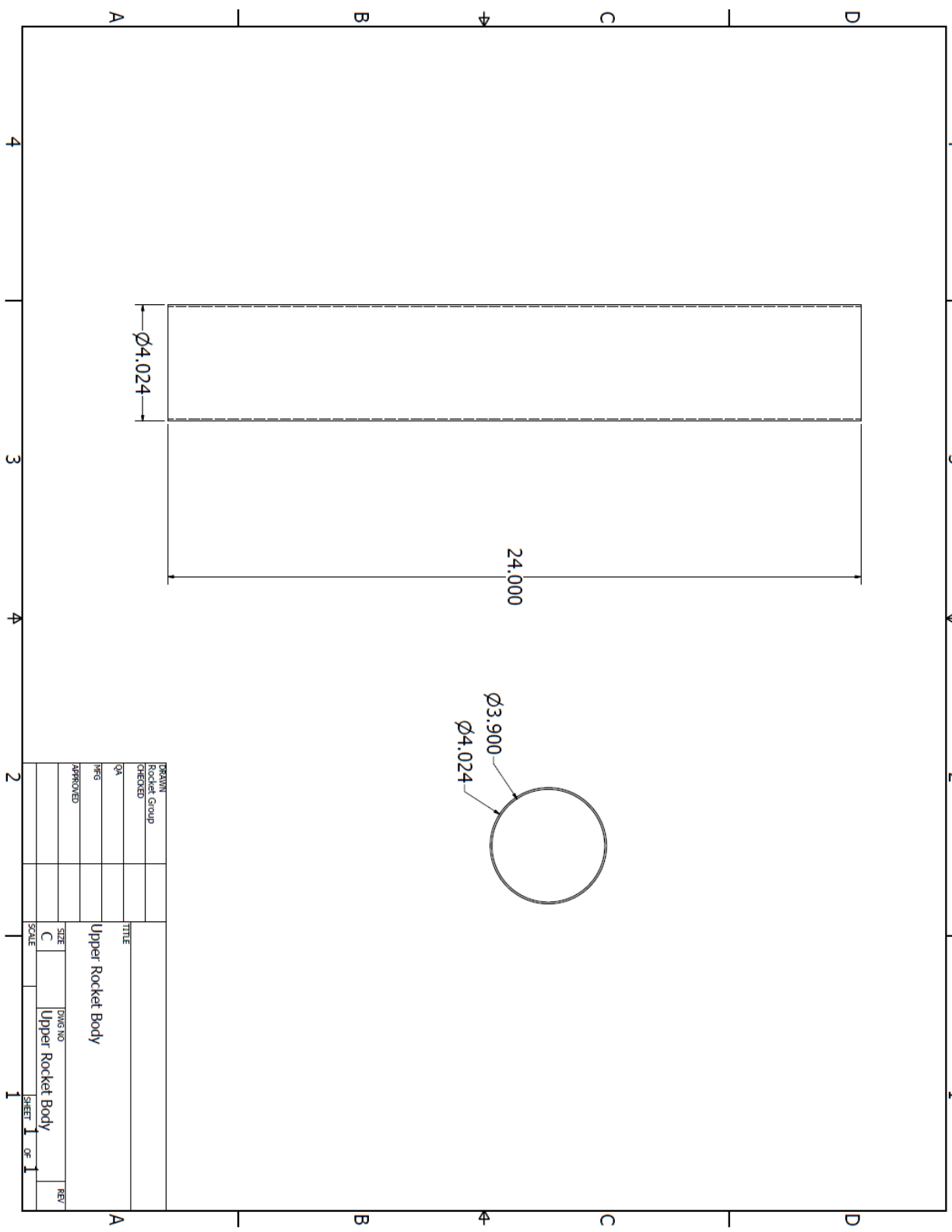

Figure A1.4: Upper Rocket Body

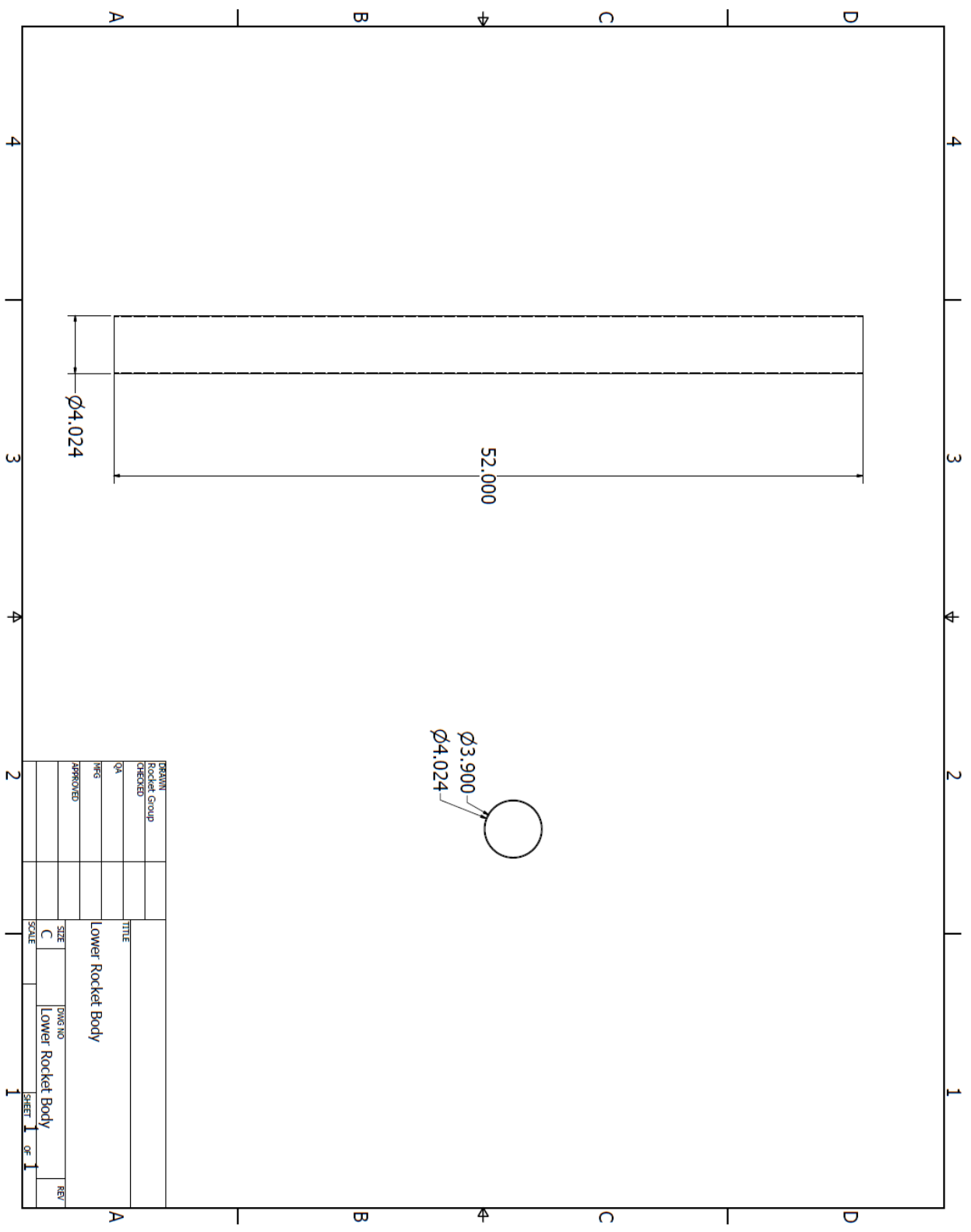

Figure A1.5: Lower Rocket Body

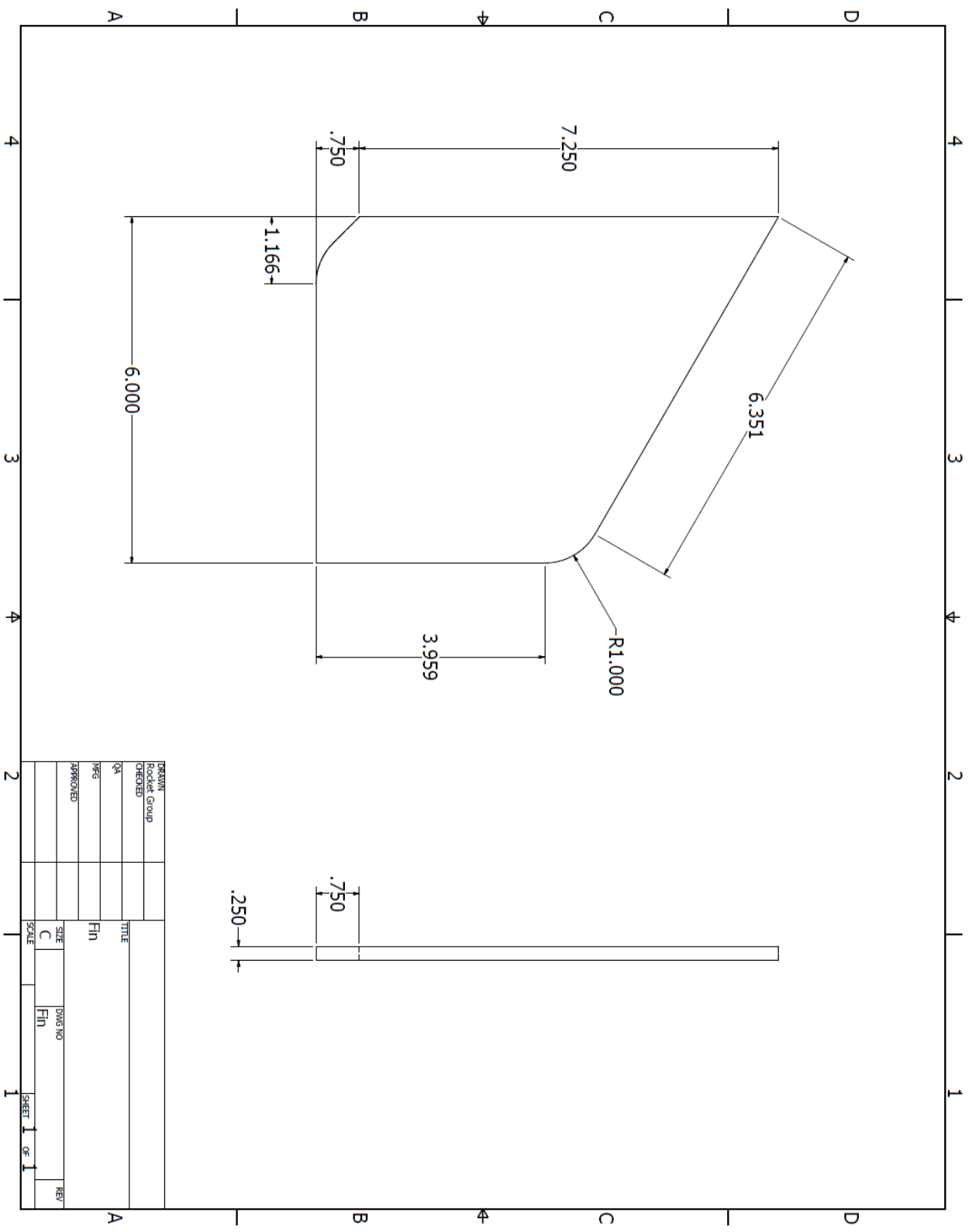

Figure A1.6 Rocket Fin

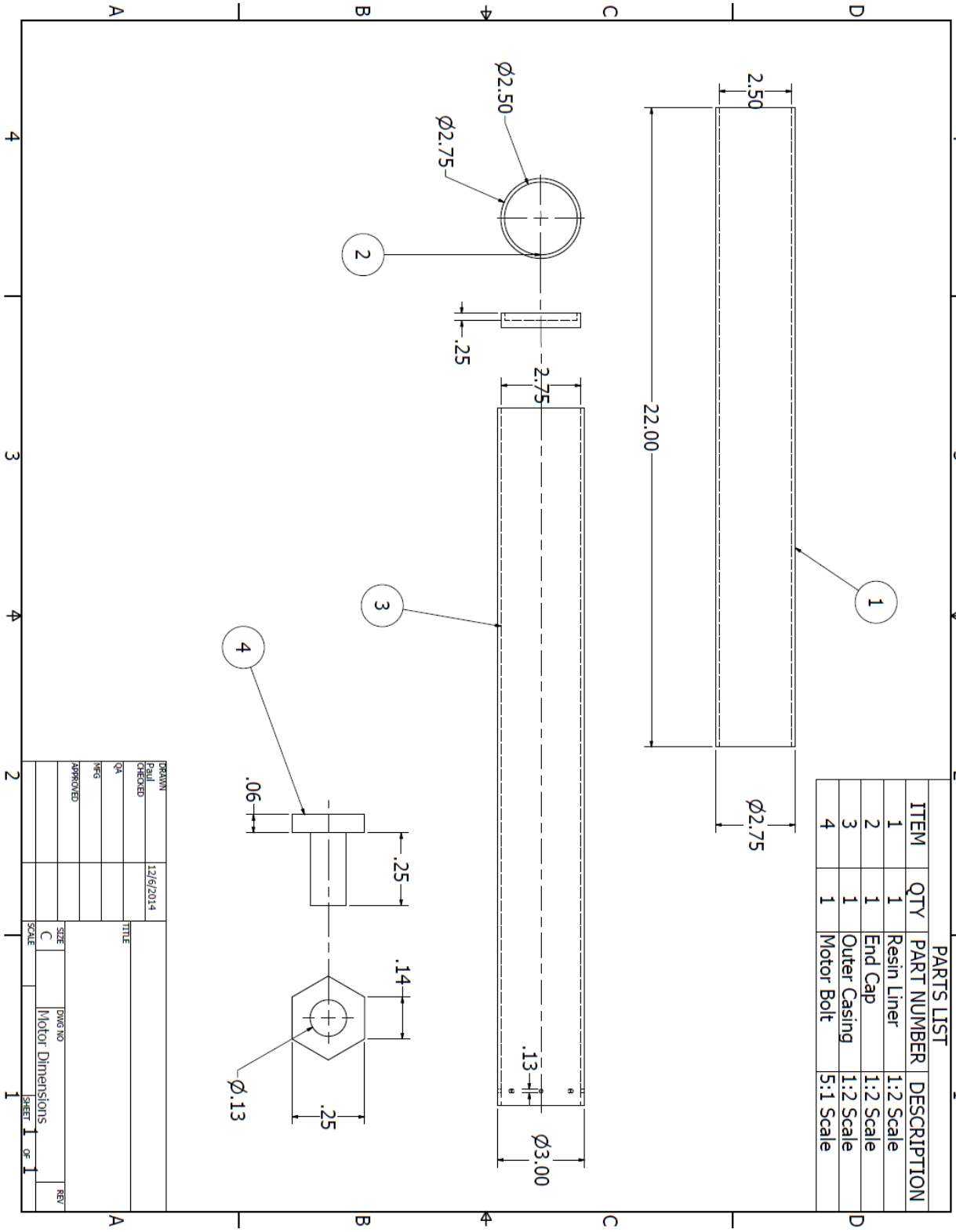

Figure A1.7: Rocket Motor Dimensions

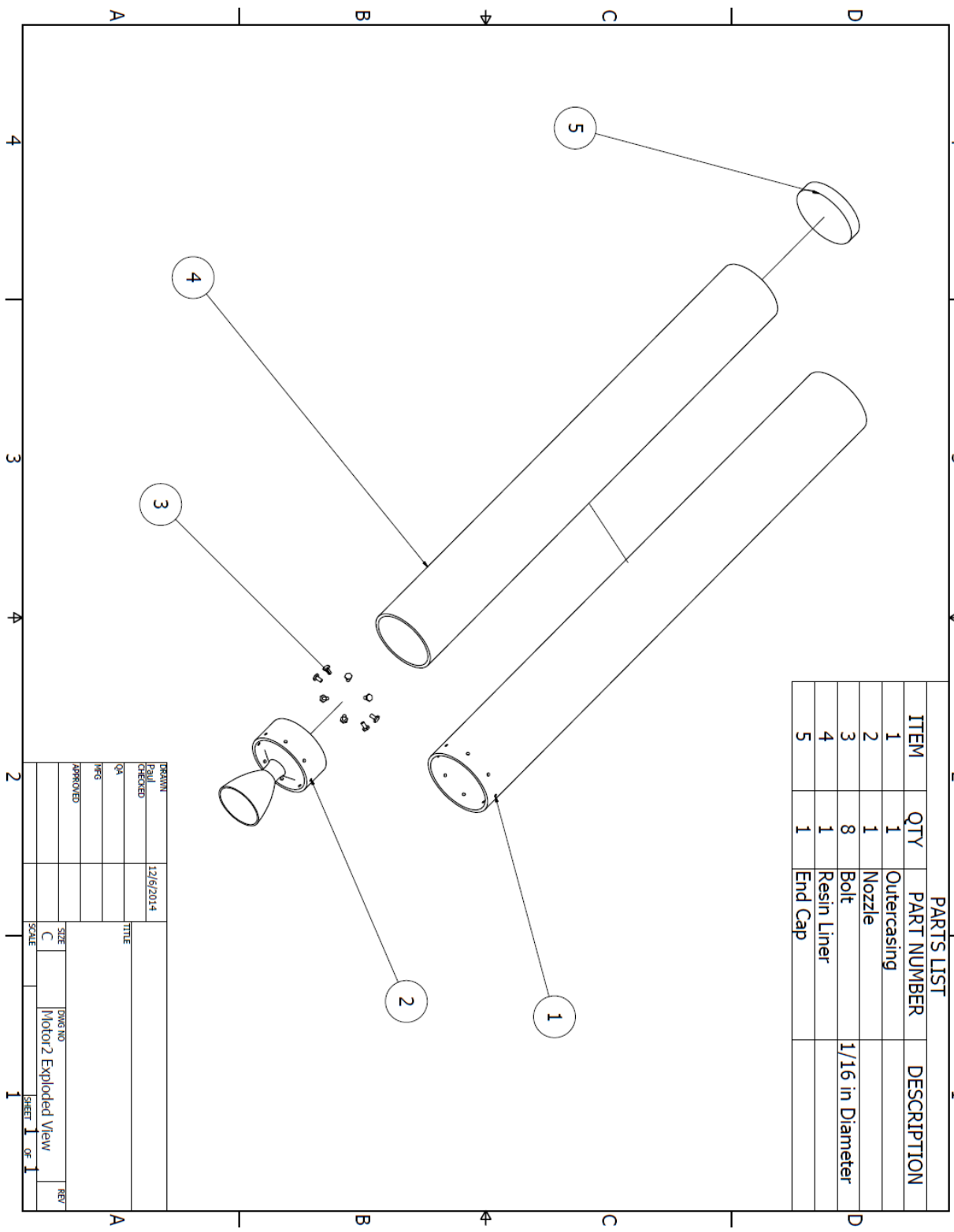

Figure A1.8: Rocket Motor Components

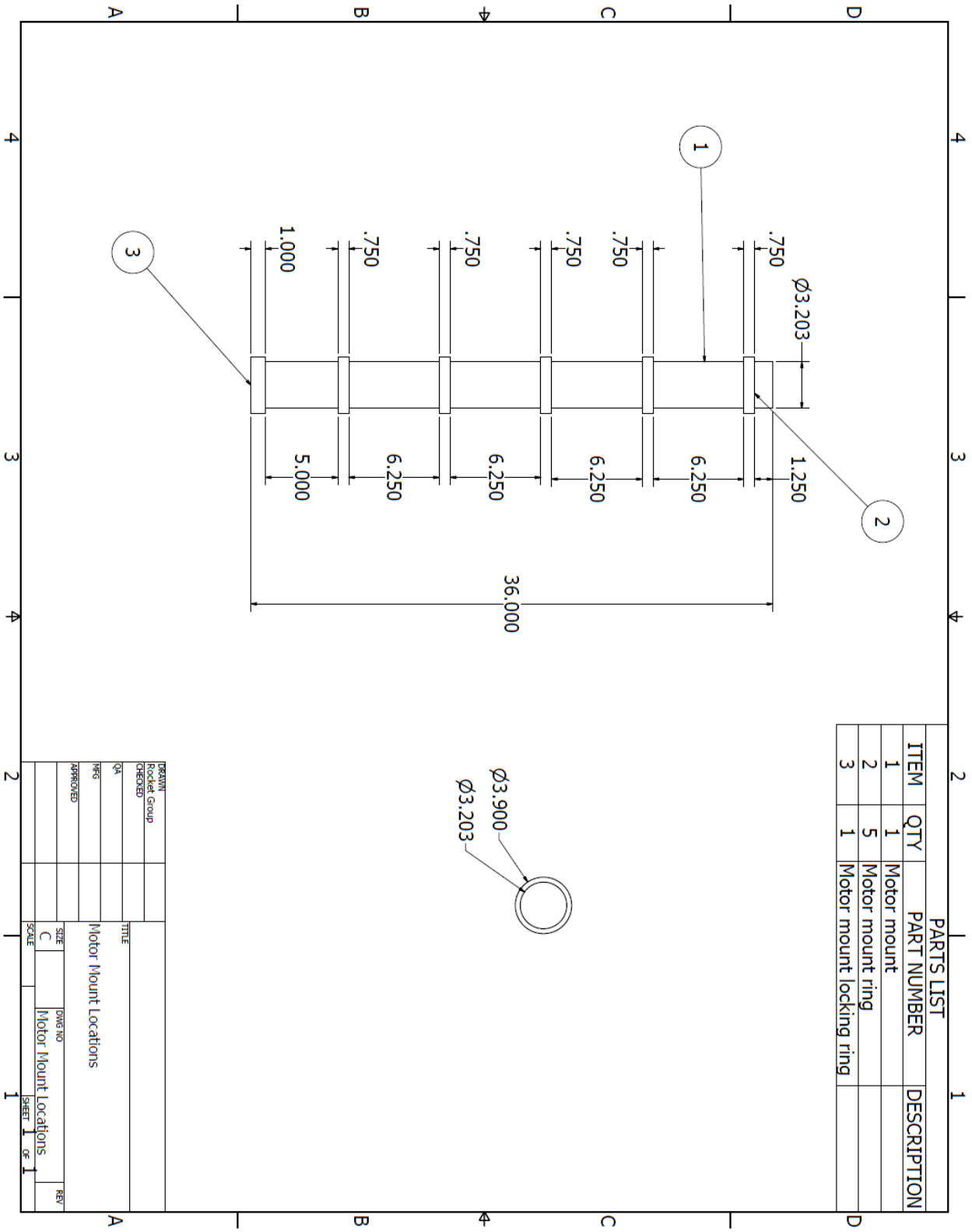

Figure A1.9: Motor Mount

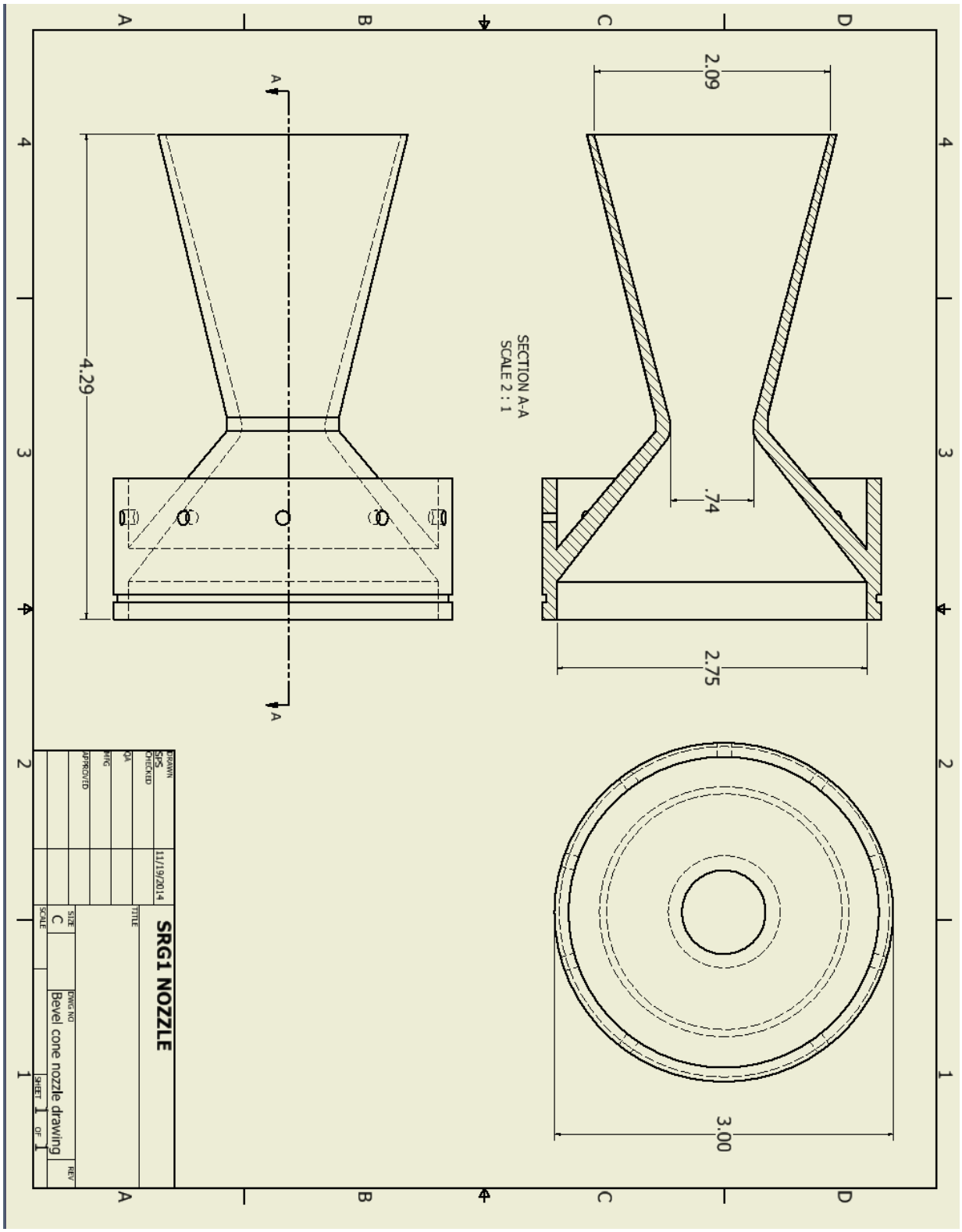

Figure A1.10: Nozzle Cone

Appendix 2: Tables

	Parameter		Units
Isp	Specific Impulse, ideal	164	sec.
Isp	Specific Impulse, measured	137	sec.
C*	Characteristic exhaust velocity, theoretical	2993 (912)	ft/s (m/s)
C*	Characteristic exhaust velocity, measured	2922 (891)	ft/s (m/s)
To	Combustion temperature, theoretical @1000 psia	1437 (1710)	deg Celsius (K)
	Density, ideal	1.879	gram/cu.cm.
	Density, as cast	1.859	gram/cu.cm.
X	Mass fraction of condensed-phase products	0.425	-
k	Ratio of specific heats	1.043	-
M	Effective molecular wt. of exhaust products	42.39	g/mole
	Burn rate behavior	plateau	
ro	Burn rate @ 1 atm.	0.084	in/sec
r	Burn rate @ 1000 psia	0.509	in/sec
Tcr	Auto-ignition temperature	> 300	deg. C.

Table A2.1: Published Values for Potassium Nitrate-Dextrose Fuel

Appendix 3: Budget and Budget Analysis

Rocket Project Budget							
	Activity	Name of Activity Lead	Work Hours	Labor $ Rate	Labor Costs	Material Costs	Total Cost
	Design Phase						
1	Design Rocket Outer Body	Michael Wm	32	50	1600	0	1600
2	Design Rocket Test Stand	Paul	24	25	600	0	600
3	Design Payload Section	Chris	48	25	1200	0	1200
4	Design Electronics Section	Chris	80	25	2000	0	2000
5	Design Recovery Systems	Nathan	72	25	1800	0	1800
6	Design Propulsion System	Brian	84	25	2100	0	2100
7	Conduct Fuel Analyses	Michael Wb	84	25	2100	0	2100
8	Conduct Finite Element Analysis	Paul	32	25	800	0	800
9	Conduct Computational Fluid Dynamics Analysis	Charles	112	25	2800	0	2800
10	Prepare Design Report (class work included)	Nathan	400	25	10000	0	10000
	Build Phase						
11	Fabricate and Assemble Rocket and Fuel	Brian	125	125	15625	2710.67	18335.67
12	Fabricate and Assemble Rocket Test Stand	Brian	32	125	4000	861.45	4861.45
	Test Phase						
13	Wind Tunnel Testing	Chad	24	25	600	0	600
14	Test Engine Thrust	Michael Wb	45	25	1125	0	1125
15	Test Recovery System	Nathan	56	25	1400	0	1400
16	Perform Test Launch	Brian	56	25	1400	0	1400
17	**Perform Real Launch**	Brian	8	25	200	0	200
	Total:		1314		49350	3572.12	52922.12

	Breakdown of Budget by Week												
	Week												
	TBC	1	2	3	4	5	6	7	8	9	10	11	12
Design	25000	2200	2550	1950	1750	1350	2950	3510	2160	2260	2460	1460	200
Build	23198	0	0	0	0	0	0	0	0	0	0	0	0
Test	4525	0	0	0	0	0	0	0	0	0	0	0	0
Launch	200	0	0	0	0	0	0	0	0	0	0	0	0
Total	52923	2200	2550	1950	1750	1350	2950	3510	2160	2260	2460	1460	200
Cumulative Budgeted		2200	4750	6700	8450	9800	12750	16260	18420	20680	23140	24600	24800
Cumulative Actual		1147	2328.25	4398.5	5673.5	6804.75	8467.25	9492.25	10942.25	12179.75	13142.25	14254.75	15279.75
Cumulative Earned		1900	4150	5800	7250	8300	10950	13796	15292	16538	17104	17670	17790
Cost Performance Index		1.6565	1.7825	1.3186	1.2779	1.2197	1.2932	1.4534	1.3975	1.3578	1.3015	1.2396	1.1643
Cost Variance		753	1821.75	1401.5	1576.5	1495.25	2482.75	4303.75	4349.75	4358.25	3961.75	3415.25	2510.25
	Week												
	TBC	13	14	15	16	17	18	19	20	21	22	23	24
Design	25000	200	0	0	0	0	0	0	0	0	0	0	0
Build	23198	0	0	11599	11599	0	0	0	0	0	0	0	0
Test	4525	0	0	0	0	0	0	0	0	0	495	495	495
Launch	200	0	0	0	0	0	0	0	0	0	0	0	0
Total	52923	200	0	11599	11599	0	0	0	0	0	495	495	495
Cumulative Budgeted		25000	25000	36599	48198	48198	48198	48198	48198	48198	48693	49188	49683
Cumulative Actual		16479.75	NA	NA	NA	NA	NA	NA	NA	NA	NA	NA	NA
Cumulative Earned		18410	NA	NA	NA	NA	NA	NA	NA	NA	NA	NA	NA
Cost Performance Index		1.1171	NA	NA	NA	NA	NA	NA	NA	NA	NA	NA	NA
Cost Variance		1930.25	NA	NA	NA	NA	NA	NA	NA	NA	NA	NA	NA
	Week												
	TBC	25	26	27	28	29	30	31	32	33	34	35	
Design	25000	0	0	0	0	0	0	0	0	0	0	0	
Build	23198	0	0	0	0	0	0	0	0	0	0	0	
Test	4525	120	120	0	350	350	350	350	0	700	700	0	
Launch	200	0	0	0	0	0	0	0	0	0	200	0	
Total	52923	120	120	0	350	350	350	350	0	700	900	0	
Cumulative Budgeted		49803	49923	49923	50273	50623	50973	51323	51323	52023	52923	52923	

At Week Thirteen (Current Week)	
Cumulative Budgeted Cost	25000
Cumulative Actual Cost	16479.75
Cumulative Earned Value	18410
Cost Performance Index=CEV/CAV	1.1171
Cost Variance=CEV-CAV	1930.25
Forecasted Cost at Completion (TBC/CPI)	47374.13
To-Complete Performance Index=(TBC-CEV)/(TBC-CAV)	0.9470

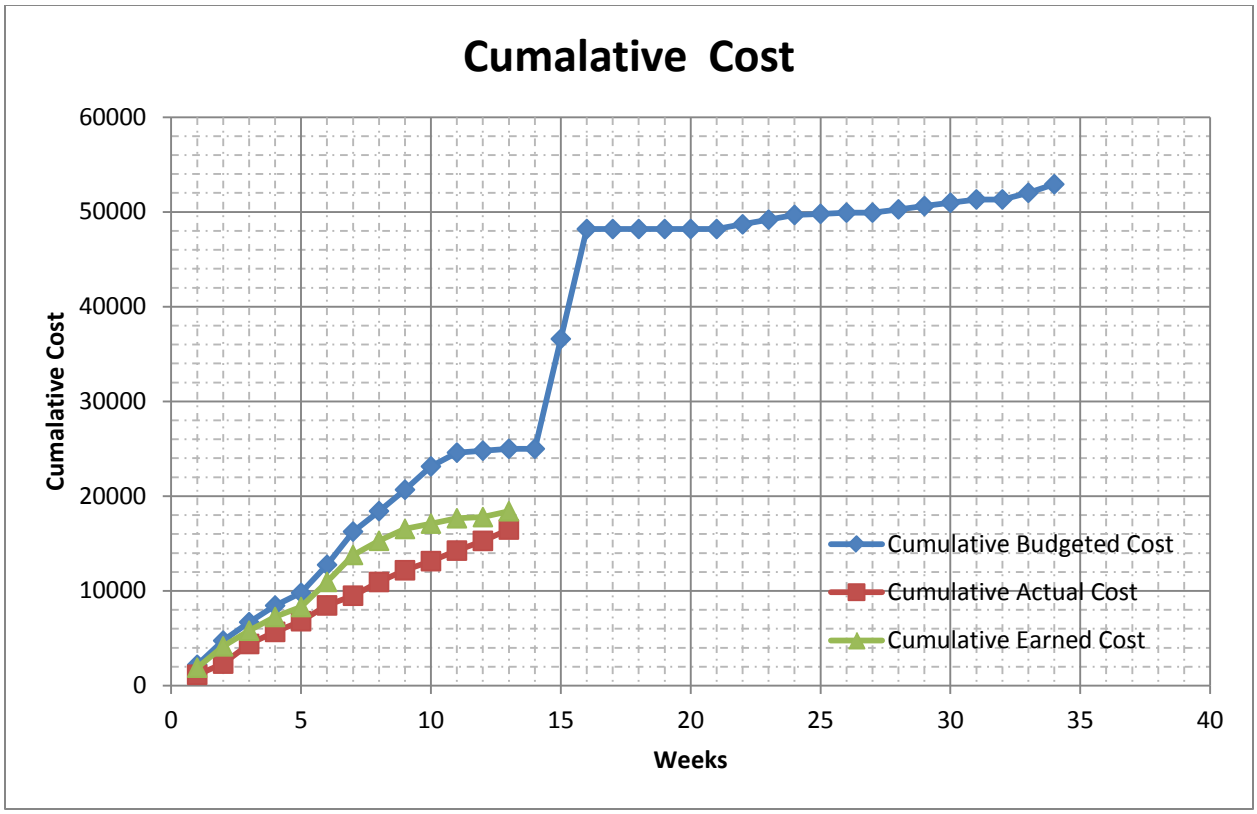

Figure A4.1: Cumulative Cost vs Weeks

The cumulative actual cost is well below the cumulative budgeted cost for week thirteen. However, this is deceptive because the cumulative earned cost is also below the cumulative budgeted cost. Not as much work was completed as was expected by week thirteen. The reason the cumulative actual cost is much lower than the cumulative budgeted cost is because the initial budget overestimated the actual project costs. The estimated cost at completion reflects this because it is slightly less than $6,000 below the cumulative budgeted cost at completion.

To get back on track, the team will be doing more work during December and January. There was weeks of slack included in the build phase to account for shipping times while the actual construction was estimated to only take one or two weeks.

Appendix 4: Gantt Chart

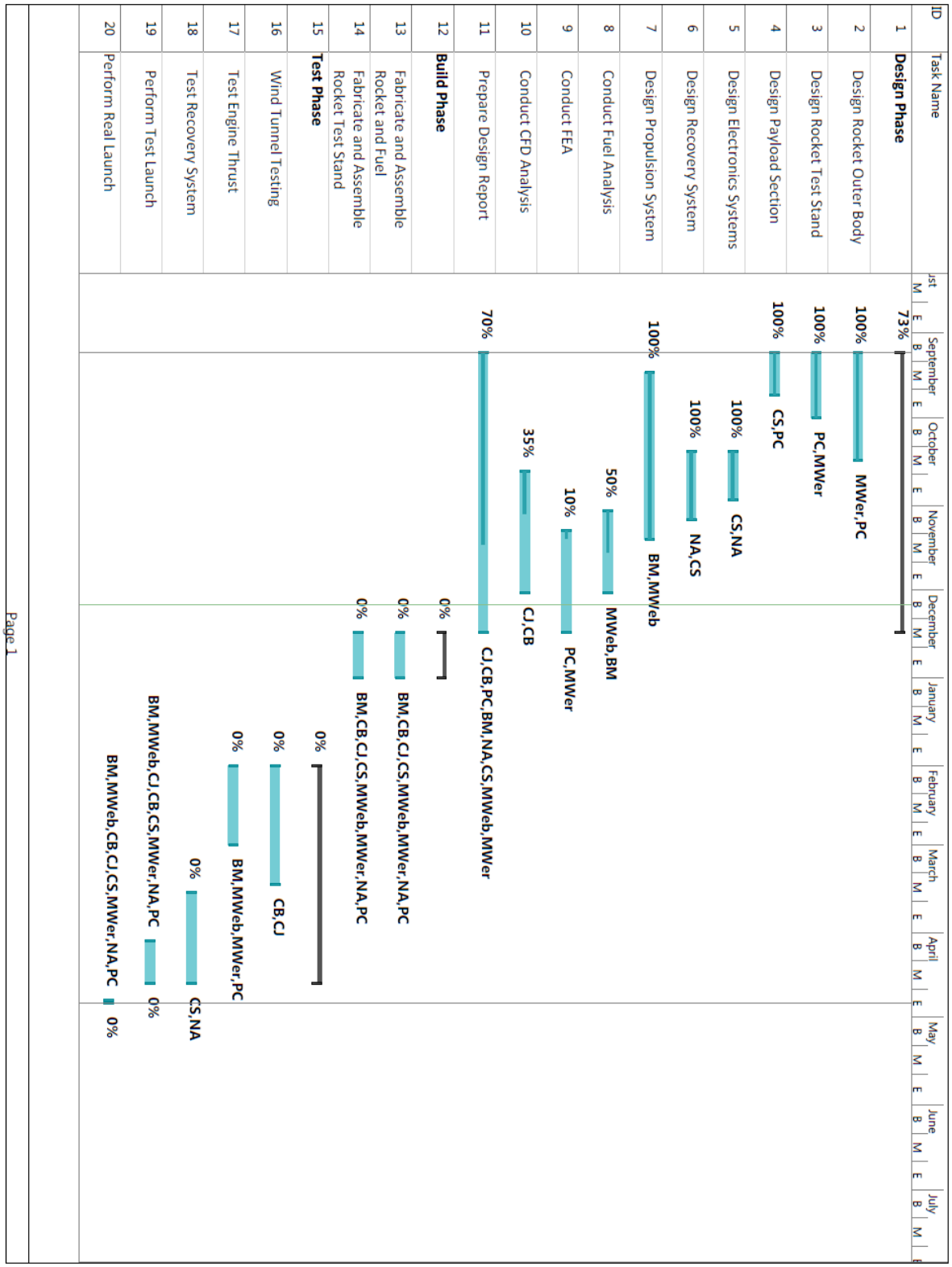

References:

[1] W. A. D. Michael T. Heath, "Virtual Prototyping of Solid Propellant Rockets," *Computer Science & Engineering*, vol. 2, pp. 21-32, 2002.

[2] J. Dues, "Avoiding finite element analysis errors," in *113th Annual ASEE Conference and Exposition, 2006, June 18, 2006 - June 21, 2006*, Chicago, IL, United states, 2006, p. Dassault Systemes; HP; Lockheed Martin; IBM; Microsoft; et al.

[3] J. F. Dues Jr, "Stress analysis for novices using autodesk inventor," in *2006 ASME International Mechanical Engineering Congress and Exposition, IMECE2006, November 5, 2006 - November 10, 2006*, Chicago, IL, United states, 2006.

[4] W. Younis, "CHAPTER 9 - The Stress Analysis Environment," in *Up and Running with Autodesk Inventor Simulation 2011 (Second edition)*, W. Younis, Ed., ed Oxford: Butterworth-Heinemann, 2010, pp. 235-275.

[5] S. Ping, "Dynamic Modeling and Analysis of a Small Solid Launch Vehicle," in *Information Engineering and Computer Science*, 2010.

[6] T. Benson, "Specific Impulse," NASA Glenn Research Center, 12 June 2014. [Online]. Available: http://www.grc.nasa.gov/WWW/K-12/airplane/specimp.html. [Accessed 3 November 2014].

[7] T. V. Radovich, "Performance of materials in solid propellant rocket motor exhaust environments," in *14th Intersociety Conference on Environmental Systems, July 16, 1984 - July 19, 1984*, San Diego, CA, United States, 1984.

[8] K. Ramaswamy, M. Buragohain, and B. S. Rao, "Design and development of composite rocket motor casing," *Journal of Aerospace Quality and Reliability*, vol. 1(6), I pp. 11-18, 07/ 2005.

[9] P. Thakre, R. Rawat, R. Clayton, and V. Yang, "Mechanical erosion of graphite nozzle in solid-propellant rocket motor," *Journal of Propulsion and Power,* vol. 29(3), pp. 593-601, 05/ 2013.

[10] B. Broquere, M. Dauchier, C. Just, J.-C. Tricot, and J. H. Koo, "Advances in heat resistant materials for solid rocket motors and heat shields," in *58th International Astronautical Congress 2007, September 24, 2007 - September 28, 2007*, Hyderabad, India, 2007, pp. 5073-5086.

[11] K.-Y. Hwang and Y.-J. Yim, "Effects of propellant gases on thermal response of solid rocket nozzle liners," *Journal of Propulsion and Power,* vol. 24(4), pp. 814-821, 2008.

[12] H. He, "Some essential problems of ablation and heat-conduction in solid rocket nozzle," *Tuijin jishu,* pp. 22-28, 35, 1993.

[13] N. F. Krasnov Ed, V. N. Koshevoy, A. N. Danilov, and V. F. Zakharchenko, "Rocket aerodynamics," 1971.

[14] J. P. Reding and L. E. Ericsson, "Hammerhead and nose-cylinder-flare aeroelastic stability revisited," *Journal of Spacecraft and Rockets,* vol. 32(1), pp. 55-59, 1995.

[15] A. Fedaravicius, S. Kilikevicius, and A. Survila, "913. Optimization of the rocket's nose and nozzle design parameters in respect to its aerodynamic characteristics," *Journal of Vibroengineering,* vol. 14(4), pp. 1885-1891, 2012.

[16] J. Morote and G. Liano, "Flight dynamics of unguided rockets with free rolling wrap around tail fins," in *43rd AIAA Aerospace Sciences Meeting and Exhibit, January 10, 2005 - January 13, 2005*, Reno, NV, United states, 2005, pp. 7061-7074.

[17] J. Simmons, A. Deleon, J. Black, E. Swenson, and L. Sauter, "Aeroelastic analysis and optimization of FalconLAUNCH sounding rocket fins," in *47th AIAA Aerospace Sciences*

Meeting including the New Horizons Forum and Aerospace Exposition, January 5, 2009 - January 8, 2009, Orlando, FL, United states, 2009.

[18] J. T. Ross, M. R. Risbeck, R. J. Simmons, A. J. Lofthouse, and J. T. Black, "Experimental fin tips for reusable launch vehicles (ExFiT) flight data validation," in *52nd AIAA/ASME/ASCE/AHS/ASC Structures, Structural Dynamics and Materials Conference, April 4, 2011 - April 7, 2011*, Denver, CO, United states, 2011.

[19] National Aeronautics and Space Administration (NASA). (2014). *Beginner's Guide to Model Rockets/Forces on a Rocket* [Online]. Available: http://exploration.grc.nasa.gov/education/rocket/rktfor.html

[20] R. Nakka, "KN - Dextrose Propellant," Richard Nakka's Experimental Rocketry Web Site, 15 July 2006. [Online]. Available: http://www.nakka-rocketry.net/dex.html. [Accessed 19 November 2014].

[21] R. Nakka, " KN-Dextrose Propellant Chemistry and Performance Characteristics," Richard Nakka's Experimental Rocketry Web Site, 10 December 2000. [Online]. Available: http://www.nakka-rocketry.net/dexchem.html. [Accessed 19 November 2014].

[22] R. Nakka, " Rocketry Software," Richard Nakka's Experimental Rocketry Web Site, 18 October 2014. [Online]. Available: http://www.nakka-rocketry.net/softw.html. [Accessed 19 November 2014].

[23] J. S. DeMar, "The Propellant:Nozzle Area Ratio - A Practical Guide to Kn," ThrustGear.Com, 2 February 2007. [Online]. Available: http://www.thrustgear.com/topics/Kn_Notes.htm. [Accessed 3 November 2014].

[24] AltusMetrum. (2014). *TeleMetrum* [Online]. Available: http://altusmetrum.org/TeleMetrum/

[25] T. Apke. (2014, Nov.1). *Black Powder Usage* [Online]. Available: http://www.info-central.org/?article=303

[26] E. K. Huckins, "Snatch force during lines-first parachute deployments," *Journal of Spacecraft and Rockets*, vol. 8, pp. 298-9, 1971.